Sub-10-attosecond Path-length Stabilisation using Phase-locked Spectral Interferometry

Jack Morse[1,3], Pedro Oliveira[1*], Alexander Aiken[2], Marco Galimberti[1]

[1*]Central Laser Facility, STFC, Rutherford Appleton Laboratory, Harwell, OX11 0QX, United Kingdom.
[2]Accelerator Science and Technology Centre (ASTeC), STFC, Daresbury Laboratory, Warrington, WA4 4AD, United Kingdom.
[3]University of Bath, Claverton Down, Bath, BA2 7AY, United Kingdom.

*Corresponding author(s). E-mail(s): pedro.oliveira@stfc.ac.uk;
Contributing authors: jack.morse2001@gmail.com; alexander.aiken@stfc.ac.uk; marco.galimberti@stfc.ac.uk;

Abstract

Path-length stabilisation down to the femtosecond level and below is a crucial challenge for next-generation laser facilities, particularly when pump-probe configurations demand femtosecond delays between pulses on target. We present a proof-of-principle linear technique for attosecond level path-length stabilisation using spectral interferometry. Advantages of this technique include its cost-effectiveness, low power requirements, compatibility with a wide variety of laser sources, no restriction on pulse duration, and delay monitoring over a large temporal range. We demonstrate drift-free operation over a 24-hour period with total integrated jitter reduced to a remarkable 6.8 attoseconds between 1 mHz – 625 Hz, with an average power of 25 μW. The sensitivity of the system has been characterised to 91.91 mV/fs.

Keywords: Spectral interferometry, Path-length stabilisation, Timing, Synchronisation

1 Introduction

Spectral interferometry (SI), a linear optical technique involving the combined interference of two pulses in the spectral domain, has a wide range of applications in optics [1–7]. A vast amount of information is contained in the spectral phase difference between the pulses, such as the time delay or difference in dispersion experienced between the two arms. The latter allows SI to be widely used in dispersion measurements of optical fibres or other dispersive media, through a method known as Fourier transform spectral interferometry (FTSI) [8, 9]. Here, we use the methods' high sensitivity to changes in time delay to lock the path-length difference between two independent arms down to the attosecond level.

For next-generation laser facilities, experimenters are demanding femtosecond delays between pulses in pump-probe configurations, to explore more extreme and ultra-fast interactions. Such forthcoming examples are for instance Vulcan 20-20 [10] or ELI facilities [11], which will have several petawatt (PW) level ultra-fast lasers with their arrival time precisely controlled in a target chamber. Other science facilities, such as the MEC

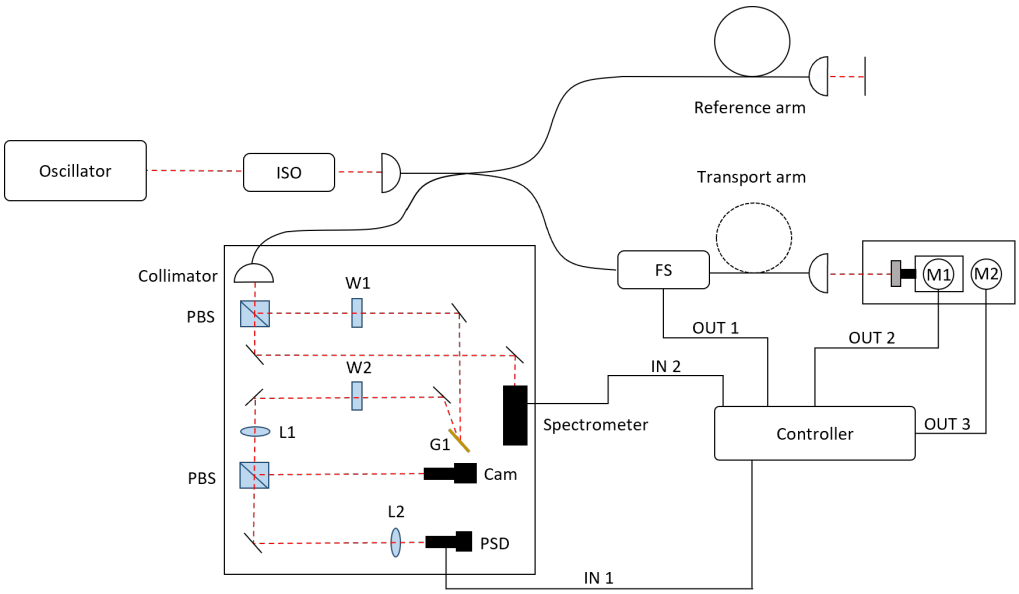

Fig. 1: Experimental setup. W1 and W2 are $\lambda/4$ waveplates; G1 is a 1200 lines/mm reflective diffraction grating; L1 a +150 mm lens; L2 a +25.4 mm lens; FS is the fibre stretcher; M1 a voice coil actuator; M2 a stepper motor; PSD a position sensing device, ISO is an optical isolator, PBS is a polarisation beam-splitter.

LCLS [12] upgrade and CLARA-FEBE, will have high-intensity lasers combined with other sources of coherent light.

Therefore, the control of independent optical paths (OP) is an active area of interest. To achieve these requirements, temporal stabilisation of OPs must be at least an order of magnitude better than the demands, which for a 10 fs delay would correspond to fixing path lengths to within 0.3 μm over the entire beam path. For facilities with longer optical paths, this challenge becomes practically harder to maintain due to higher environmental fluctuation amplitudes.

Without active stabilisation, on target delays can reach sub-picosecond depending on the total propagation distance, but this is limited by the natural fluctuations due to temperature and acoustic noise along the beam path. The origin of these fluctuations makes them typically low frequency ($\lesssim$ 100 Hz), but they can be many kHz. For finer control of the delay, active stabilisation cannot be ignored.

The most sensitive of these methods for path-length stabilisation is the OXC; these work on the principle of overlapping two pulses on a nonlinear crystal, where the difference intensity of the second harmonic on two photodiodes gives a measure of the pulse overlap. A feedback loop can then be used to keep the difference value constant, thus locking the delay between the pulses. However, as this technique uses a nonlinear process it requires relatively high powers and short pulse durations. Further, if timing is lost in this method (i.e. there is no second harmonic signal on the photodiodes), which only occurs in a very small window of size comparable to the sum of the FWHMs of the pulses, it can be challenging to re-establish the zero-timing.

In this article, we present a proof-of-principle method of OP stabilisation method by spectral interferometry in an in-fibre interferometer where the total propagation in each arm was approximately 70 m. Compared to the OXC approach, which is sensitive to changes in the arrival of the pulse envelope, spectral interferometry goes a step further: it is sensitive to changes at the optical cycle level, i.e. it is inherently more timing sensitive. This method also has the advantage of timing monitoring over a much larger temporal window as SI occurs even outside of direct pulse overlap.

In Section 2 we present the method, along with the necessary calibrations, the experimental setup, and in Section 3 we present our long and short-term stabilisation results.

2 Methods

As shown schematically in Fig. 1, our experimental setup was constructed on a single optical bench and consisted of an in-fibre Michelson interferometer with the light approximately 50:50 split through each arm. The fibre used was HI1060 single mode (SM) fibre and the laser was a 1040 nm-centered 20 nm bandwidth 80 MHz source. The OP was stabilised in the transport arm through two components: An in-line fibre stretcher (FS) for fast delay compensation and a voice coil (M1) to adjust for slow drifts. The retro-mirror M1 at the end of the transport arm was mounted on a ThorLabs stepper motor for rough timing adjustment.

Both arms of the interferometer nominally have the same total fibre propagation of 70 m, with an uncertainty of 1%. After being retro-reflected, the pulses are recombined at the fibre splitter, with some of the light entering the diagnostic setup; the rest of the light is blocked by an optical isolator. Our diagnostics consisted of a commercial spectrometer and a custom fast spectrometer with a position sensor device (PSD) as a detector and a camera for alignment. The commercial spectrometer provided the range for monitoring and rough alignment, whilst the fast spectrometer signal was used in a PID loop to lock the delay between the pulses. The grating G1 was imaged at a line focus onto first the camera with a 7 nm field of view (FOV), and second the PSD with a 2 nm FOV, equal to the size of the interference fringe we chose to lock to.

Stabilisation Scheme

Stabilisation between the paths was achieved through locking the chosen fringe on the PSD (model PDP90A from Thorlabs) in a two-level PID feedback loop which was tuned [13]. The bandwidth of the PSD was quoted at 15 kHz and set the response rate of the system. The output voltage of the first loop was split, with one part amplified and sent to the FS and the other part becoming the input to the second loop, with its output being sent to M1. The second loop compensates for slow drifts and ensures the output of the fast loop remains close to the zero set-point, thus increasing the speed of the response. The output voltages in each loop were scaled by a gain value obtained through calibrations. The FS (model PZ1-SM4-PC-E-980 from Optiphase) had a range of 14 μm and high bandwidth, making it suitable for a low amplitude, high-frequency delay compensation. M1 could compensate for a much larger range of delays (up to 20 picoseconds) but with a lower bandwidth, around 1 kHz. M1 also had a known resonance at approximately 25 Hz, however, this did not noticeably affect the operation and could be suppressed through damping or selecting an alternative device in future work.

Theoretical model

Consider the spectral interference $S(\lambda)$ between the recombined pulses with a difference in spectral phase $\Delta\varphi$ due to the difference in propagation in each arm, which for two Gaussian pulses is given by

$$S(\lambda) = \left(|E(\lambda)| \cos\left(\frac{\Delta\varphi(\lambda)}{2} \right) \right)^2 , \qquad (1)$$

where the $|E(\lambda)|$ is the spectral envelope and the cosine of the difference in spectral phase describes the interference.

The spectral phase difference is simply the difference in phase accumulated due to different propagation paths. We considered a small difference in the index of refraction Δn_f between the fibres in the two arms, a fixed difference in fibre length ΔL_f (responsible for the characteristic interferogram profile – see Fig. 2), and difference in air propagation ΔL_{air}, so that

$$\Delta\varphi = \frac{2\pi}{\lambda} \left(\Delta L_f \overline{n}_f + \overline{L}_f \Delta n_f + \Delta L_{air} \right) , \qquad (2)$$

where $\overline{L}_f$ is the mean fibre path length of the two arms. The zero-delay wavelength, by definition, exists when the delay between a single wavelength in the combined pulses is zero – these appear as inflexions in the interference spectrum. The spectral phase difference was well approximated as quadratic, meaning there was only a single zero-delay wavelength, which occurred at $\lambda = \lambda_0$ when

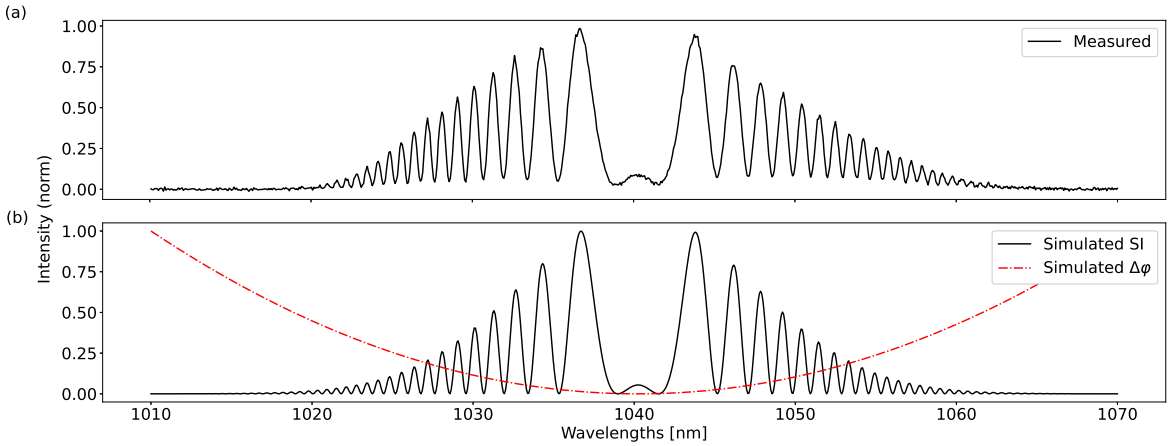

Fig. 2: (a) Measured spectral interference compared with (b) the simulated interference of two Gaussian pulses of equal intensity with 10 nm bandwidth and $\Delta\varphi = 0.27852\ [\mathrm{nm}^{-2}] \cdot(\lambda - 1040.2\ [\mathrm{nm}])^2 + 2.7$ rad.

$d\Delta\varphi/d\lambda = 0$. It follows under this condition, by differentiating and rearranging Eq. 2,

$$\Delta L_{air} = -\Delta L_f \overline{n}_g - \overline{L}_f \Delta n_g \qquad (3)$$

is required. Therefore, controlling ΔL_{air} controls the zero-delay wavelength in the spectrum.

Further, for small changes in delay, such that the zero-delay wavelength does not measurably shift, a phase change in the spectrum still occurs, provides information about the delay, and is extractable for calibration of the system. It was necessary to obtain calibrations for each loop independently so the effectiveness of the system could be translated to a real time delay and assessed. We performed the two calibrations and present the results in the *Calibration* subsection.

Calibration

For the fast loop during operation, we had access to the voltage output of the PSD. To convert this to delay values, we find a calibration in delay per Volt. This was achieved by varying the set-point voltage of the fast loop and recording the spectrum. Fig. 3 (b) shows how over the 60 mV range where a lock to a common fringe was maintained, the phase of the spectrum changed.

To extract the delay from the phase of the spectrum, we performed a fit using a quadratic expansion of the phase in the form

$$\Delta\varphi \simeq \beta(\lambda - \lambda_0)^2 + \delta \qquad (4)$$

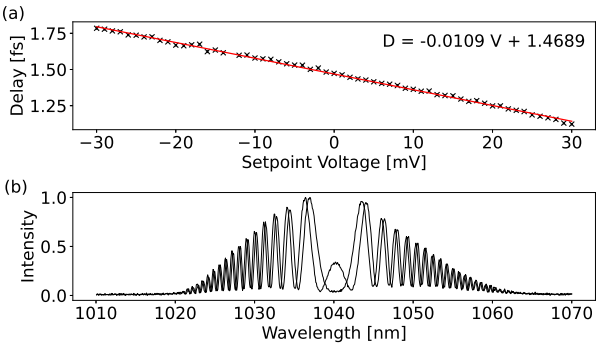

Fig. 3: The change in phase extracted from the spectra for varying set-point voltages in the PID loop driving the FS was converted to delay and plotted. The resulting fit gives a time calibration of 10.9 as/mV. The lower plot shows the maximum phase change over the set-point range –30 mV to +30 mV.

where $\beta = (1/2)(\partial^2\Delta\varphi/\partial\lambda^2|_{\lambda=\lambda_0})$ here is proportional to the group delay dispersion (GDD) and is independent of the delay, λ_0 is the zero-delay wavelength and δ is an additional phase term.

Fig. 2 demonstrates the results of an independent fit which was used to determine the β and λ_0 for this dataset: $\beta = 0.27852\ \mathrm{nm}^{-2}$ and $\lambda_0 = 1040.2$ nm; these were used as a seed in the minimisation procedure to ensure fast and accurate convergence of the fits to the data. As

expected, the only parameter to vary in our optimisation was δ, which changed linearly, describing the change in phase as the set-point varied.

To relate this change in phase to a real delay, we derive the relation

$$\frac{d\Delta\varphi}{d\tau} = \frac{2\pi c}{\lambda_0}, \tag{5}$$

which shows that a change in phase of 2π directly corresponds to a time delay of T between the two pulses, where T is the optical period of the zero-delay wavelength. Using this, we converted the extracted phases to real delays, and the results are presented in Fig. 3 (a), yielding a calibration of 10.9 as/mV, corresponding to a sensitivity of 91.91 mV/fs. This allows us to quantify the stability of the fast loop, as demonstrated in Section 3.

For larger delay changes with a measurable shift in the zero-delay wavelength, a similar calibration to relate the zero-delay wavelength to the change in time delay was performed. The relation derived for this was

$$\frac{d\lambda_0}{d\tau} = \frac{\pi c}{2\lambda_0^2}\beta^{-1}. \tag{6}$$

According to Eq. 6 introducing a delay τ results in a shift in the zero-delay wavelength of 3.1 nm/ps. In practice, we adjusted the motor M2 in micrometer increments while monitoring λ_0 with the stabilisation loops turned off. This calibration, illustrated in Fig. 4, yielded a value of 2.8 nm/ps, which is in good agreement with the expected value.

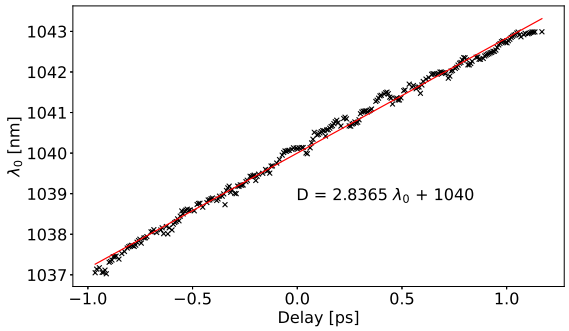

Fig. 4: Change in location of λ_0 as the delay is changed by varying M2 in micrometer steps. The relation is linear and shows the change in λ_0 in the spectrum with respect to time $d\lambda_0/dt = 2.8$ nm/ps.

3 Results

To demonstrate the long-term operation of the system, we ran a 24 hour test monitoring the spectrum and extracting λ_0 both with and without the stabilisation running. The results of this are summarised in Fig. 5. From this, a measurement of the peak-to-peak natural variation in delay between the two fibres over this period was 1.3 ps. However, with the loops running not only was λ_0 unchanging, but the phase of the spectral interference remained locked for the full 24 hour period.

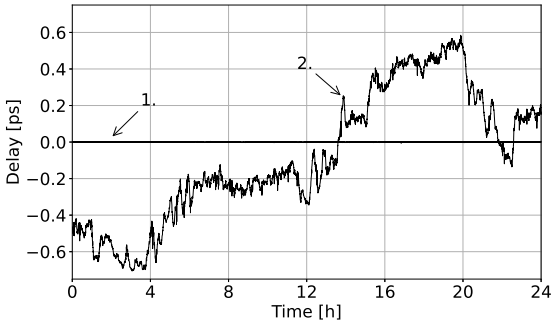

Fig. 5: 1. Over 24 hours we can see no drift at the picosecond scale to the system. 2. When unstabilised the delay between the fibres can be seen to change of the order of 1.3 picoseconds.

To better characterise the setup with the active stabilisation running, we performed three tests.

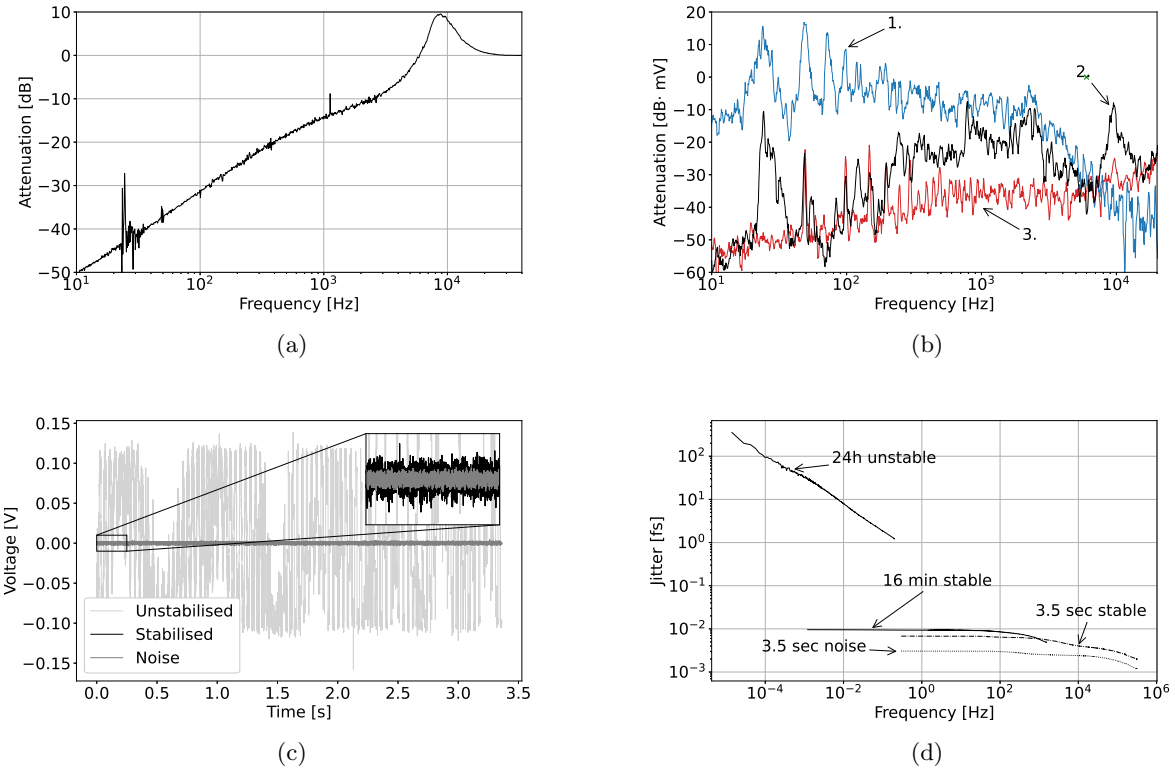

Fig. 6: (a) Attenuation of a signal at each frequency. The spike at 25 Hz is a resonant line, known to come from the voice coil device (M1). (b) 1. Frequency amplitudes of the unstabilised signal 2. The attenuation of each frequency when the system is being stabilised 3. A measurement of the electrical noise of the sensor. (c) Voltage output signal from the PSD over short time period of 3.5 s with 3.2 μs sampling interval. (d) The integrated jitter up to the Nyquist frequency for the unstabilised, stabilised and noise signals. The total integrated jitter for the stabilised signal is 6.8 as.

First, a lock-in amplifier was used to input a signal into the loop at frequencies ranging from 10 Hz to 40 kHz and the attenuation of this signal was measured. In Fig. 6a we can see a high level of attenuation which linearly decreases up to higher frequencies. The line seen at 25 Hz is the known resonance line of the voice coil, which is essentially a speaker (see Thorlabs' website for details).

Next, we measured the attenuation of the system for each frequency, for the three cases: stabilisation of both loops running, stabilisation off, and laser off to measure the electrical noise of the PSD. In practice, the measurements of unstabilised signals are really an underestimate of the true instability, as the fringe movement on the sensor is larger than the sensor itself. However, we can see in Fig. 6b the effectiveness of the stabilisation relative to the electrical noise of the sensor. Other than the resonant line at 25 Hz (due to the voice coil), which is suppressed but not eliminated, the stabilisation up to 100 Hz is indiscernible from the noise, which is an attenuation corresponding to five orders of magnitude. For higher frequencies, we still see suppression up to 6 kHz, with some amplification after this, consistent with the results seen in Fig. 6a.

For the final characterisation, we measured the total timing jitter for a single pass of the system. We took measurements of the voltage output of the PSD on a short time scale (3.5 seconds) with a sampling interval of 3.2 μs and medium time scale (16 minutes) with a sampling interval of 0.8 ms. Fig. 6c shows how close to the noise the

system was capable of stabilising to. We then performed an integrated jitter calculation (Fig. 6d), giving the jitter up to a given frequency. Up to the Nyquist frequency we measure for the 3.5 second trace a total jitter in phase delay N_ϕ of 2.9 attoseconds (integrated between 0.3 Hz and 156 kHz), and for the 16 minute trace a total jitter of 6.8 attoseconds (integrated between 1 mHz and 625 Hz). As we are locking the phase, this jitter corresponds to the variation as a result of the phase velocities in the recombined pulses. For a corresponding jitter in terms of the group delay N_g between the two pulses we use the following formula

$$N_g = \left(1 - \lambda \frac{\overline{n}_f'}{\overline{n}_f}\right)\Bigg|_{\lambda=\lambda_0} N_\phi, \tag{7}$$

which is derived from relating the phase and group delays to the change in fibre path length. By assuming the mean refractive index of the fibre is fused silica, we yield the constant of proportionality in Eq. 7 to be very close to unity, and so the group delay jitter is actually indiscernible from the phase jitter.

We expect that these results will translate with larger fibre lengths and unwrapping the transport fibre, as this should only introduce low frequencies from temperature and acoustic fluctuations which we have demonstrated this system is effective at suppressing.

4 Conclusion

We have demonstrated the suitability of SI as an alternative technique applied to path-length stabilisation. In particular, we have shown that SI is remarkably sensitive both at measuring and compensating delay changes at the attosecond level.

By constructing an in-fibre interferometer we used a fibre-stretcher and movable mirror to change the delay in one arm through a two-level feedback loop. By locking the phase of the interference spectrum, we were able to fix the delay between the two interferometer arms. Through the necessary calibrations we were able to quantify both the sensitivity of the system and its performance. With the phase-lock running, we measured the total integrated jitter between 1 mHz and 625 Hz to be 6.9 as, and demonstrated this lock could be maintained over an extended period of 24 hours.

The main advantages of this system are its cost-effectiveness, lack of restrictions on optical power and pulse duration, and its ease to realign after zero-timing is lost. We anticipate that such a system can be extended to a laser facility as the frequency of environmental fluctuations should not change considerably, only their amplitude, however further investigation into this will be required.

References

[1] Oksenhendler, T., Coudreau, S., Forget, N., Crozatier, V., Grabielle, S., Herzog, R., Gobert, O., Kaplan, D.: Self-referenced spectral interferometry. Applied Physics B **99**(1), 7–12 (2010) https://doi.org/10.1007/s00340-010-3916-y . Accessed 2024-03-07

[2] Zhong, Z., Zhang, L., Jiang, H., Gu, H., Chen, X., Zhang, C., Liu, S.: Improved Fourier transformation based method for accurate phase and amplitude retrieval in spectral interferometry. Journal of Optics **22**(3), 035501 (2020) https://doi.org/10.1088/2040-8986/ab6a69 . Publisher: IOP Publishing. Accessed 2024-03-07

[3] Börzsönyi, A., Kovács, A.P., Görbe, M., Osvay, K.: Advances and limitations of phase dispersion measurement by spectrally and spatially resolved interferometry. Optics Communications **281**(11), 3051–3061 (2008) https://doi.org/10.1016/j.optcom.2008.02.002 . Accessed 2024-03-07

[4] Kovács, A.P., Osvay, K., Kurdi, G., Görbe, M., Klebniczki, J., Bor, Z.: Dispersion control of a pulse stretcher– compressor system with two-dimensional spectral interferometry. Applied Physics B **80**(2), 165–170 (2005) https://doi.org/10.1007/s00340-004-1706-0 . Accessed 2024-03-07

[5] Schlichting, S., Willemsen, T., Ehlers, H., Morgner, U., Ristau, D.: Fourier-transform spectral interferometry for in situ group delay

dispersion monitoring of thin film coating processes. Optics Express **24**(20), 22516–22527 (2016) https://doi.org/10.1364/OE.24.022516 . Publisher: Optica Publishing Group. Accessed 2024-03-07

[6] Bowlan, P., Gabolde, P., Shreenath, A., McGresham, K., Trebino, R., Akturk, S.: Crossed-beam spectral interferometry: a simple, high-spectral-resolution method for completely characterizing complex ultrashort pulses in real time. Optics Express **14**(24), 11892–11900 (2006) https://doi.org/10.1364/OE.14.011892 . Publisher: Optica Publishing Group. Accessed 2024-03-07

[7] Lepetit, L., Chériaux, G., Joffre, M.: Linear techniques of phase measurement by femtosecond spectral interferometry for applications in spectroscopy. JOSA B **12**(12), 2467–2474 (1995) https://doi.org/10.1364/JOSAB.12.002467 . Publisher: Optica Publishing Group. Accessed 2024-03-07

[8] Meshulach, D., Yelin, D., Silberberg, Y.: White light dispersion measurements by one- and two-dimensional spectral interference. IEEE Journal of Quantum Electronics **33**(11), 1969–1974 (1997) https://doi.org/10.1109/3.641311 . Conference Name: IEEE Journal of Quantum Electronics. Accessed 2024-03-07

[9] Takeda, M., Ina, H., Kobayashi, S.: Fourier-transform method of fringe-pattern analysis for computer-based topography and interferometry. JOSA **72**(1), 156–160 (1982) https://doi.org/10.1364/JOSA.72.000156 . Publisher: Optica Publishing Group. Accessed 2023-11-27

[10] Chekhlov, O., Collier, J., Clark, R.J., Hernandez-Gomez, C., Lyachev, A., Matousek, P., Musgrave, I.O., Neely, D., Norreys, P.A., Ross, I., Tang, Y., Winstone, T.B., Wyborn, B.E.: The 10 PW OPCPA Vulcan laser upgrade. In: CLEO/Europe - EQEC 2009 - European Conference on Lasers and Electro-Optics and the European Quantum Electronics Conference, pp. 1–1 (2009). https://doi.org/10.1109/CLEOE-EQEC.2009.5196350 . https://ieeexplore.ieee.org/document/5196350 Accessed 2024-03-07

[11] Rus, B., Bakule, P., Kramer, D., Korn, G., Green, J.T., Nóvak, J., Fibrich, M., Batysta, F., Thoma, J., Naylon, J., Mazanec, T., Vítek, M., Barros, R., Koutris, E., Hřebíček, J., Polan, J., Baše, R., Homer, P., Košelja, M., Havlíček, T., Honsa, A., Novák, M., Zervos, C., Korous, P., Laub, M., Houžvička, J.: ELI-Beamlines laser systems: status and design options. In: High-Power, High-Energy, and High-Intensity Laser Technology; and Research Using Extreme Light: Entering New Frontiers with Petawatt-Class Lasers, vol. 8780, pp. 265–276. SPIE, ??? (2013). https://doi.org/10.1117/12.2021264 . https://www.spiedigitallibrary.org/conference-proceedings-of-spie/8780/87801T/ELI-Beamlines-laser-systems-status-and-design-options/10.1117/12.2021264.full Accessed 2024-03-07

[12] Dyer, G., Fry, A.: Matter in Extreme Conditions Upgrade (Conceptual Design Report). Technical Report SLAC-R-1152; MECU-DR-0003, SLAC National Accelerator Laboratory (SLAC), Menlo Park, CA (United States) (October 2021). https://doi.org/10.2172/1866100 . https://www.osti.gov/biblio/1866100 Accessed 2024-03-07

[13] Ang, K.H., Chong, G., Li, Y.: PID control system analysis, design, and technology. IEEE Transactions on Control Systems Technology **13**(4), 559–576 (2005) https://doi.org/10.1109/TCST.2005.847331 . Conference Name: IEEE Transactions on Control Systems Technology. Accessed 2024-03-07